

# UNSTEADY ROTOR AERODYNAMICS AND ACOUSTICS

M. Kuntz, R. Heinrich, K. Pahlke, J. Raddatz

DLR, Institute of Design Aerodynamics  
Lilienthalplatz 7, 38108 Braunschweig, Germany

## Abstract

An aeroacoustic method for noise prediction of helicopter rotors in forward flight is presented. The unsteady aerodynamic flow field is computed using an Euler solver for arbitrary moving coordinate systems and flexible grids taking into account the prescribed rigid blade motion. Using the computed pressure data as input, two acoustic methods are applied, on one side the linear part of the acoustic analogy method and on the other side the Kirchhoff method.

First for the 4-bladed ONERA/ECF 7AD rotor in high-speed forward flight ( $\mu = 0.4$ ) the blade pressure data computed with the present method is compared with experimental data and numerical results of other authors using e.g. Chimera method. A good overall agreement can be stated.

For the same ONERA/ECF 7AD rotor test conditions defined in the HELISHAPE project are applied ( $\mu = 0.33$ ). The comparison of computed pressure data with the experimental data is less satisfactory than for the first test case.

The acoustic evaluation for the second test case demonstrates, that for in-plane microphones the negative peak pressure is almost independent on the rotor thrust. For microphones out of the rotor plane, a more accurate noise prediction is obtained with lifting flow conditions by prescribing the correct blade motion at the aerodynamic computation instead of non-lifting flow conditions.

The overall differences to the experimental data are caused by the following facts. Applying the Kirchhoff method with a rotating integration surface, for the present conditions at moderate high-speed forward flight not all non-linear effects can be included inside the Kirchhoff surface. The Kirchhoff method with a non-rotating integration surface requires sufficiently accurate aerodynamic data, which cannot be obtained on the grid used due to insufficient clustering of grid points.

Presented at the 23rd European Rotorcraft Forum, Dresden, Germany, 16-18 September 1997

## Introduction

The aim of helicopter noise reduction requires the development of advanced computational methods. Annoying noise of helicopter has impulsive character and is either high-speed impulsive (HSI) noise or blade-vortex interaction (BVI) noise. The present paper concentrates on the numerical simulation of HSI noise. Most of the simulation methods are split in two parts, on one side aerodynamic codes for the computation of the acoustic sources generated by the rotor blades and on the other side acoustic codes for the prediction of noise propagation to the farfield.

Especially for the aerodynamic flow field computation the methods differ by the computational effort, accuracy and flexibility. For unsteady computations of rotors in forward flight, wake capturing methods like Chimera or overset grid methods (Pahlke and Raddatz [1], Ahmad and Duque [2]) or the moving grid approach (Boniface et al. [3], Boniface and Pahlke [4]) have been developed.

Experimental studies have shown that for HSI noise predictions for microphones located in the plane of the rotor the maximum peak pressure value is independent on the rotor thrust (Schmitz et al. [5]). Therefore, most of the aeroacoustic computations of high-speed impulsive noise from lifting helicopter rotors in forward flight are carried out by simulating non-lifting conditions. No wake capturing algorithm or wake models are included in this case (Strawn et al. [6]). For microphones not located in the rotor plane, non-symmetric blade loadings have to be considered by applying wake capturing methods or aerodynamic methods coupled to a wake-model.

The acoustic methods applied are on one side linear methods (monopole and dipole term of the acoustic analogy method) and the Kirchhoff method, which allows to include non-linear effects. For test cases in the transonic regime studies comparing these methods were carried out (Kuntz [7], Brentner et al. [8]). Both methods agree well for conditions below the delocalization Mach number, but accurate noise predictions at higher Mach numbers require the use of the Kirch-

hoff method.

One example for a combined aerodynamic and acoustic method using the overset grid technique is published by Ahmad et al. [9]. The purpose of the present work is to show the feasibility of a combined aeroacoustic method including an Euler solver using flexible grids. This paper contains first results of computations on coarse grids. For a high-speed forward flight test case ( $\mu = 0.4$ ) defined by ONERA for the ONERA/ECF 7AD rotor comparisons of aerodynamic blade pressure data with experiments (Beaumier et al. [10]) and Euler results computed by other authors using different methods (e.g. Chimera) are carried out.

Furthermore this paper shows comparisons of aeroacoustic computations with experimental data for the ONERA/ECF 7AD rotor measured in the DNW in the framework of the HELISHAPE program (Schultz et al. [11]). For this moderate high-speed forward flight test case with  $\mu = 0.33$  aerodynamic and acoustic comparisons are done.

### Aerodynamic Methods

The DLR aerodynamic code FLOWer is applied for the computation of the present test cases. FLOWer is a finite-volume solver for the solution of the Navier-Stokes equations on arbitrary moving coordinate systems and flexible grids (Kroll et al. [12]). In the framework of the present work only inviscid computations are carried out. The integral form of the three-dimensional Euler equations in a moving Cartesian coordinate system can be written as:

$$\frac{\partial}{\partial t} \int_V \vec{W} dV + \int_{\partial V} \vec{F} \cdot \vec{n} dS + \int_V \vec{G} dV = 0 \quad (1)$$

with

$$\begin{aligned} \vec{F} &= \begin{bmatrix} \rho \\ \rho u \\ \rho v \\ \rho w \\ \rho E \end{bmatrix}, \\ \vec{F} &= \begin{bmatrix} \rho (\vec{q} - \vec{q}_b) \\ \rho u (\vec{q} - \vec{q}_b) + p \vec{e}_x \\ \rho v (\vec{q} - \vec{q}_b) + p \vec{e}_y \\ \rho w (\vec{q} - \vec{q}_b) + p \vec{e}_z \\ \rho E (\vec{q} - \vec{q}_b) + p \vec{q} \end{bmatrix}, \\ \vec{G} &= \begin{bmatrix} 0 \\ \rho (\vec{\omega} \times \vec{q})_x \\ \rho (\vec{\omega} \times \vec{q})_y \\ \rho (\vec{\omega} \times \vec{q})_z \\ 0 \end{bmatrix} \end{aligned} \quad (2)$$

$\vec{W}$  is the vector of conservative quantities with  $\rho$ ,  $\vec{q}$  and  $E$  denoting the density, absolute velocity vector referred to the blade fixed coordinate system and specific total energy, respectively.  $V$  denotes an arbitrary deforming control volume with boundary  $\partial V$  and the outer normal  $\vec{n}$ . A source term  $\vec{G}$  has to be added, including the time derivatives of the unit base vectors of the coordinate system rotating with the angular velocity  $\vec{\omega}$ . The gas is assumed to behave like a calorically perfect gas with constant specific heats.

For the calculation of the convective flux tensor  $\vec{F}^c$  the boundary velocity  $\vec{q}_b$  has to be introduced. This vector is defined in the moving frame and contains three components induced through translation, rotation of the coordinate system and the deformation of the mesh (compare figure 1):

$$\vec{q}_b = \vec{q}_{trans} + \vec{q}_{rot} + \vec{q}_{flex} \quad (3)$$

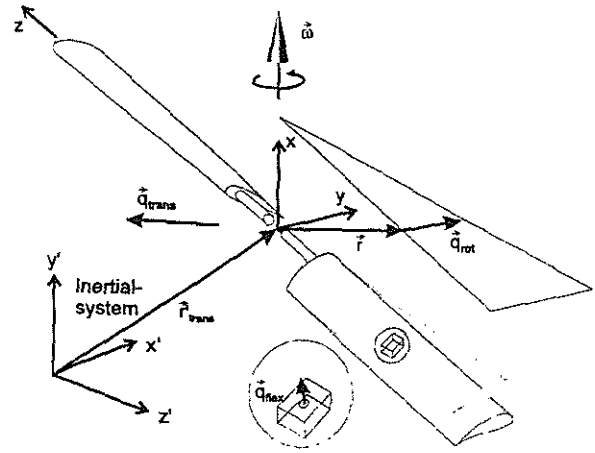


Figure 1: Moving coordinate system

The translational velocity is determined by the advance direction of the rotor and the tilt of the rotor plane according to the tip path plane angle  $\alpha_{TPP}$  and is obtained by the free stream velocity in the inertial system  $\vec{q}'_{trans}$  by:

$$\vec{q}_{trans} = \overline{D}^{-1} \vec{q}'_{trans} \quad (4)$$

The rotational velocity is defined by:

$$\vec{q}_{rot} = \vec{\omega} \times \vec{r} \quad (5)$$

with the angular velocity:

$$\begin{aligned} \vec{\omega} &= \dot{\psi} \begin{pmatrix} \cos \beta \cdot \cos \vartheta \\ -\cos \beta \cdot \sin \vartheta \\ \sin \beta \end{pmatrix} \\ &+ \dot{\beta} \begin{pmatrix} \sin \vartheta \\ \cos \vartheta \\ 0 \end{pmatrix} + \dot{\vartheta} \begin{pmatrix} 0 \\ 0 \\ 1 \end{pmatrix} \end{aligned} \quad (6)$$

$\alpha$ ,  $\beta$  and  $\nu$  are the azimuthal angle, flapping angle and pitching angle, respectively. Finally the deforming grid velocity is given by the local velocity for each grid point:

$$\vec{q}_{fl,r} = \dot{x}\vec{e}_x + \dot{y}\vec{e}_y + \dot{z}\vec{e}_z \quad (7)$$

The transformation between moving frame  $\vec{r}$  and the inertial frame  $\vec{r}'$  is described by:

$$\vec{r}' = \vec{r}'_{trans} + \overline{\overline{D}}\vec{r} \quad (8)$$

$\overline{\overline{D}}$  is the tensor including the rotation around three axis. For the present application of helicopter rotors in forward flight the pitching and flapping angle are periodic functions of the azimuthal angle:

$$\begin{aligned} \nu &= \nu_o + \nu_c \cos \psi + \nu_s \sin \psi \\ \beta &= \beta_o + \beta_c \cos \psi + \beta_s \sin \psi \end{aligned} \quad (9)$$

The approximation of the governing equations follows the method of lines, which decouples the discretization of space and time (Jameson et al. [13]). The spatial discretization is based on a finite volume method which subdivides the flow field into a set of non-overlapping hexahedral cells. The cell-vertex approach is realized, in which the flow variables are associated with the vertices of the cell. The spatial discretization leads to a system of ordinary differential equations for the rate of change of the conservative flow variables in each grid point. The time integration is realized using the Dual-Time-Stepping method according to Jameson [14] implemented in FLOWer. This method has been already applied to other unsteady test cases (Heinrich et al. [15]).

The no-normal flow condition is imposed on a body. The far field boundary is treated following the concept of characteristic variables for non reflecting boundary conditions (Kroll [16]). Auxiliary cells are used to store the neighbour flow values in order to match the solution across inner cuts. In order to have second order spatial accuracy at inner cuts two layers of auxiliary cells are used.

The multibladed rotor is computed by simulating all blades together without introducing special boundary conditions to take into account the influence of the other blades. Body conforming single block computational grids of an OH topology with a wraparound O in chordwise direction and the H-type in spanwise direction are generated around each blade. These grids are transformed in a cylindrical shape with an azimuthal extension of the segment of  $2\pi/N$  ( $N =$  number of blades). Finally the blocks of all blades are connected forcing an equivalent point distribution at the

connection planes. For each block, the  $I$ -index runs in the wraparound direction, the  $J$ -index in the blade normal direction and the  $K$ -index in the spanwise direction.

To take into account the relative motion of the blades, the technique of flexible grids is applied. The overall grid system is defined with zero pitching and flapping angles, the angular velocity vector according to eq. (6) is  $\vec{\omega} = \dot{\psi}\vec{e}_x$ . While the outer part (farfield) of each block is fixed in the rotating system, the inner part including the rotor blade is moving according to eq. (9) dependent on the actual azimuthal location. The outer boundary of this inner part is typically a few chord length away from the rotor blade and is given by the location of the Kirchhoff surface (compare description of the acoustic methods). Inbetween the grid is distorted linearly. Consequently, the velocity is splitted according to eq. (3) in a translational part, a rotational part without pitching and flapping (which is the same for all blades) and a deforming grid velocity dependent on the actual location of each grid point.

For the application of the acoustic methods an interface is defined. This interface allows to extract pressure data (pressure and pressure gradient) from the aerodynamic solution on planes of the aerodynamic grid (also the blade surface itself). Furthermore data can be computed on cylindrical surfaces in the flow field (including top and bottom), whereby the values at the nodes of the cylinder are obtained by a trilinear interpolation of the flow solution at the nodes of the aerodynamic grid. The pressure data is written to special files at the end of each physical time step.

### Acoustic Methods

The acoustic program system used for the present computations is called APSIM (Acoustic Prediction System based on Integral Methods). It is in principle an acoustic postprocessor for the aerodynamic solution and gives results in the form of acoustic signatures, sound pressure levels or spectra. The methods included are the linear acoustic analogy method (monopole and dipole term according to Farassat formulation I and IA) and the Kirchhoff method including the formalism with rotating and non-rotating integration surface. Parallel to these methods a routine is implemented to extract directly pressure data from the flowfield solution to allow the acoustic evaluation for microphones located inside the computational domain.

The code is based on the results of former code developments of DLR on the field of acoustic integral methods and is the basis for further code improvements. In the present code version results of the work

of Lohmann [17], Schultz et al. [18], Kuntz et al. [19] and Kuntz [7] is included.

In the framework of the present paper information is given focussed on code adaptations and extensions for the application in combination with an aerodynamic method using flexible grids. Further details about the acoustic codes is given by Kuntz [7].

The linear acoustic analogy method uses the rotating blade as integration surface. The formula for monopole and dipole are (Farassat and Succi [20], Brentner [21]):

$$P_M(\vec{x}, t) = \frac{1}{4\pi} \int_S \left[ \frac{\rho_\infty a_\infty (\dot{M}_n + \dot{n}_M)}{r(1-M_r)^2} \right]_\tau dS + \frac{1}{4\pi} \int_S \left[ \frac{\rho_\infty a_\infty M_n \dot{M}_r}{r(1-M_r)^3} \right]_\tau dS + \frac{1}{4\pi} \int_S \left[ \frac{\rho_\infty a_\infty^2 M_n (M_r - M^2)}{r^2(1-M_r)^3} \right]_\tau dS \quad (10)$$

$$P_D(\vec{x}, t) = \frac{1}{4\pi} \int_S \left[ \frac{n_r \dot{P} + \dot{n}_r P}{a_\infty r(1-M_r)^2} \right]_\tau dS + \frac{1}{4\pi} \int_S \left[ \frac{n_r \dot{M}_r P}{a_\infty r(1-M_r)^3} \right]_\tau dS + \frac{1}{4\pi} \int_S \left[ \frac{(n_r - M_n) P}{r^2(1-M_r)^2} \right]_\tau dS + \frac{1}{4\pi} \int_S \left[ \frac{n_r (M_r - M^2) P}{r^2(1-M_r)^3} \right]_\tau dS \quad (11)$$

The Kirchhoff method included in APSIM is using the formulas according to Farassat (Farassat and Myers [22], Lyrintzis [23]):

$$P(\vec{x}, t) = \frac{1}{4\pi} \int_S \left[ \frac{E_1}{r(1-M_r)} + \frac{E_2 P}{r^2(1-M_r)} \right]_\tau dS \quad (12)$$

$E_1$  and  $E_2$  are given as:

$$E_1 = M_n \vec{M} \cdot \nabla P - \vec{n} \cdot \nabla P - \frac{M_n \dot{P}}{a_\infty} + \frac{(\dot{n}_r - \dot{M}_n - \dot{n}_M) P + (n_r - M_n) \dot{P}}{a_\infty (1-M_r)} + \frac{\dot{M}_r (n_r - M_n) P}{a_\infty (1-M_r)^2} \quad (13)$$

$$E_2 = \frac{(1-M^2)(n_r - M_n)}{(1-M_r)^2} \quad (14)$$

The Kirchhoff method evaluating the integral in the rotating frame has in general a subsonically moving integration surface a few chord length away from the rotor blade. The part of the grid between the rotor blade and the Kirchhoff surface is rigidly connected with the blade and the grid adjustment to the far field is done in the outer part outside the Kirchhoff surface. Therefore, the laws for location and velocity are the same for the rotor blade and the rotating Kirchhoff surface using the actual values for  $\psi, \beta, \vartheta$  (eqs. (8), (3)). The acceleration of the integration surface is just the derivative of the rotational boundary velocity vector (compare eq. (3)).

$$\vec{q}_b = \vec{\omega} \times \vec{r} + \dot{\vec{\omega}} \times (\vec{\omega} \times \vec{r}) \quad (15)$$

For the Kirchhoff method with the non-rotating integration surface the combination with an aerodynamic code using flexible grids requires no further code adaptations, because the integration surface is defined in the wind tunnel system. The velocity is equal to the translational velocity and all acceleration terms are zero.

The acoustic integrals are computed using wind tunnel conditions. All vectors are transformed in the system of the integration surface, which is depending on the method either directly connected with the blade or non-rotating. The evaluation time level can be either the emission time or the reception time (Brentner [24]). For the application of helicopter rotors in forward flight, it is advantageous to use the emission-time-based formalism, because the pressure data has to be stored only for one time level. Furthermore the computation of the reception time for a given emission time is faster than vice versa, because at least for a rotating integration surface the movement of the microphone is simpler than the one of the acoustic sources. The acoustic pressure at a fixed observer time is obtained by a temporal interpolation of the acoustic reception time signals.

#### ONERA/ECF 7AD Rotor (S1)

The 7AD rotor was tested in the ONERA S1 wind tunnel at the Modane test center and results were published by Beaumier et al. [10]. Further details about the rotor are also given in [10]. The rotor has an aspect ratio of 15 and experimental data are given as pressure coefficients at the spanwise location of 0.5, 0.7, 0.82, 0.92 and 0.98 rotor radii. The test case chosen corresponds to a rotational tip Mach number of  $M_{\omega R} = 0.617$  with an advance ratio of  $\mu = 0.4$  and a

free stream Mach number of  $M_\infty = 0.2468$ . The rotor shaft angle is equal to  $-11.8$  degree. The following flapping and pitching motions of the blades are used for the computations (see Boniface and Pahlke [4]):

$$\begin{aligned} \beta_0 &= 11.36^\circ & \beta_c &= 1.9181^\circ & \beta_s &= -5.0778^\circ \\ \beta_0 &= 2.203^\circ & \beta_c &= -5.0778^\circ & \beta_s &= 0^\circ \end{aligned} \quad (16)$$

No hinge offset was considered for the computations. For this test case no experimental acoustic data is available, therefore no acoustic computations are carried out.

### Aerodynamic Results

The grid used for the present computation has 4 OH-blocks with 57 grid points in chordwise direction, 25 grid points in blade normal direction and 37 grid points in spanwise direction and  $57 \times 28$  points on the blade, therefore 210 900 points in total. Figure 3 shows the total block structure. To show the effect of grid distortion, 2D views are shown for grid planes with spanwise locations of about  $r/R=0.9$  and 4 azimuthal positions in figure 4.

The Dual-Time-Stepping method is used with 512 physical time steps per period and 30-50 subiterations at each step. The CPU time for one period is about 10h on a NEC SX4 vector computer.

A comparison of numerical and experimental results for the normal force coefficient at 4 radial position is presented in figure 5. The results of the current flexible grid method are given by the solid line, while the dotted and the dashed line show results which have been published by Boniface and Pahlke [4] of a DLR chimera computation and an ONERA deforming grid computation. The experimental data is given by the symbols. In figure 6 the pressure coefficient at  $r/R=0.92$  for 6 azimuthal positions is presented. The overall agreement of the prediction methods is quite good. The DLR chimera and the DLR flexible grid computations agree well with each other, whereas the ONERA deforming grid solution predicts higher  $c_n M^2$ -values. The agreement of all three numerical predictions with the experimental data is fair. All methods underpredict the  $c_n M^2$ -values for  $r/R = 0.5$  and  $\psi = 170^\circ$ . The authors believe that the high experimental normal force coefficients at this radial position are due to the fact, that the rotor support induces velocities which increase the effective pitch angle at the blade (see Schwarz [25]). For  $r/R = 0.92$  and  $r/R = 0.98$  all numerical methods predict normal force coefficients with a phase shift compared to the experimental data. The reason for this phase shift and for the overprediction of the normal force coefficient is the rigid blade assumption in the numerical simulations which is not fully valid in the tip region

of the advancing blade of this high-speed rotor.

### ONERA/ECF 7AD Rotor (DNW)

The measurements were carried out in the DNW within the HELISHAPE project, the test procedure is described by Schultz et al. [11]. Pressure data is measured at radial stations of 0.5, 0.7, 0.82, 0.92 and 0.98 rotor radii. For this test case acoustic data is available for microphones on a traverse perpendicular to the advance direction. This traverse is located about 2.5 rotor radii in front of the rotor and one rotor radius under the rotor plane. The microphones are equally spaced from  $-1.25$  to  $1.25$  rotor radii along the traverse. For the present investigation only microphone 1, 6 and additionally an in-plane microphone located above microphone 6 is considered (see figure 2). The

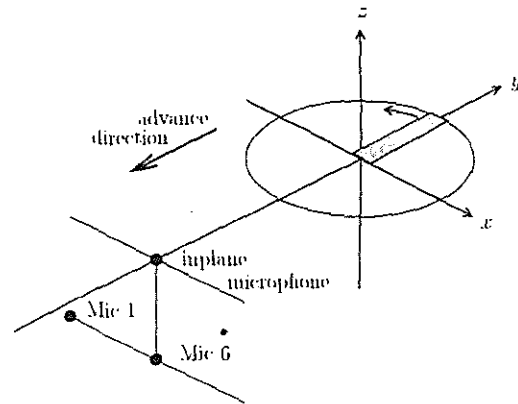


Figure 2: DNW microphone arrangement

computation was conducted using the blade motion measured at the blade root in the experiment.

Test run 142 of the DNW measurement series is chosen, which corresponds to the flight conditions  $M_{w,R} = 0.6604$ ,  $\mu = 0.3276$  and  $M_\infty = 0.2164$ . Pitching and tip path plane angles are typical for a test case with moderate high-speed level flight flow conditions. The rotor was trimmed with zero flapping.

### Aerodynamic Results

The aerodynamic computations are carried out on the same grid described already for the first test case. Figures 7 and 8 show the comparison of predicted and measured normal force coefficient and pressure coefficients respectively. The agreement between the simulation and the experiment is less favourable than for the S1 test case. The numerical simulation underpredicts at all radial positions the normal force coefficient in the range of  $60^\circ$  to  $260^\circ$ . The reason for these deviations between theory and experiment is not understood up to now. The best agreement is achieved for  $r/R=0.98$ .

Additionally non-lifting test conditions with zero pitching and flapping angles are applied for this rotor to examine the influence of the aerodynamic input data on the acoustic results. No aerodynamic results are shown, because they are intentional different to the experimental data.

### Acoustic Results

Different acoustic methods are applied to compare pressure signatures at the location of the microphones. Results of studies are shown comparing the acoustic analogy method (in the figures denoted as Far1A = Farassat formulation 1A) and the Kirchhoff method (in the figures denoted as KirchRot (rotating surface) and KirchNonrot (non-rotating surface)). The flow conditions of the present test case with an advancing tip Mach number of about 0.88 are suitable to apply both Kirchhoff formalisms. Furthermore computations using lifting or non-lifting aerodynamic input data are performed to show the influence for in-plane and out-plane microphones.

The discretization of an integration surface is determined by the aerodynamic grid in case of the rotating integration surface. The blade itself has 1596 grid points and a typical Kirchhoff surface has about 2394 points. The non-rotating cylindrical surface has 513 x 21 grid points with a clustering of points near the rotor plane. An view of the integration surfaces (two blade surfaces, two rotating Kirchhoff surfaces and a part of the non-rotating cylindrical surface) is shown in figure 9. The CPU time required for the acoustic computation of one microphone is in the order of a few seconds, therefore negligible compared to the effort for the aerodynamic computation.

In figure 10 the acoustic signatures for monopole and dipole contribution for microphone 1 (advancing side) and 6 (centerline) are compared using the following conditions. Firstly aerodynamic data of the lifting rotor is taken and the acoustic computation is evaluated using the same blade locations and velocity as for the aerodynamic computation (Euler lift/Far1A lift). The second curve (denoted as Euler lift/Far1A nonlift) uses the same input data, but neglects the pitching and flapping angles for the acoustic evaluation. The change for the acoustic pressure is quite small. Finally the aerodynamic solution of the non-lifting rotor is used as input data and zero pitching and flapping is forced for the acoustics yielding a difference in the acoustic signature (Euler nonlift/Far1A nonlift). A better agreement in peak value and temporal peak location is obtained for the aerodynamic data using the correct blade motion. The differences to the experimental data are partly due to neglecting non-linear effects, but the BVI-like pressure fluctuations found for microphone 6 are not expected for the present moderate high-speed level flight flow condi-

ons.

Before executing the same studies for the Kirchhoff method with rotating surface, the effect of different locations of the Kirchhoff surface is investigated. The results are shown in figure 11. The distance to the rotor is varied using 1, 2 or 3 chord lengths. A good agreement of the numerical results with each other and with the experimental data is found for the locations not so close to the rotor blade. In figure 12 a comparison with different aerodynamic input using the Kirchhoff method with rotating integration surface is shown. The same conclusion as for the acoustic analogy method can be drawn. The difference to the experimental data can be explained as follows. For an advancing tip Mach number of about 0.88 it is not possible to include all transonic effects inside a Kirchhoff surface, which has to be restricted to the subsonic flow regime corresponding to 1.1 rotor radii. Therefore the same discrepancies as for the linear acoustic analogy method are observed.

For the Kirchhoff method with non-rotating surface the location of the Kirchhoff surface is varied in order to find the correct location of the integration surface (Figure 13). In all cases the vertical extension of the Kirchhoff surface is 0.5 rotor radii and top and bottom part of the cylinder are included. For both microphone locations, almost identical results for both inner surface locations are obtained. For the surface far away from the rotor the peak value of the signature is decreasing and also the temporal peak location is changed. This leads to the conclusion, that the acoustic wave is not computed accurately up to the location of the Kirchhoff surface, because the aerodynamic grid is too coarse in this region. The study of the influence of lifting/non-lifting input data (figure 14) show the same tendency as for the other acoustic methods.

A summarizing result of the studies shown up to now can be seen in figure 15. The discrepancies to the experimental data have been already explained before. A further comparison of lifting and non-lifting input data is performed for an in-plane microphone using the linear acoustic analogy method. This microphone is located at the centerline in front of the rotor, one rotor radius above microphone 6. Figure 16 shows an almost constant peak pressure value. This confirms the experimental result of Schmitz et al. [5], who stated a peak pressure value independent on rotor thrust. An equivalent tendency is found applying the Kirchhoff method.

The next comparison is carried out for microphone 1 between the linear acoustic analogy method, the Kirchhoff method with a rotating surface and the experimental data. Figure 17 (left) indicates, that approximately up to the 6th harmonic the sound pressu-

re values are computed well by the numerical method. An overall comparison for all microphones along the traverse for the 1st and 6th harmonic is shown in figure 17 (right). The sound pressure levels are computed better on the advancing side ( $\psi < 180^\circ$ ) than on the retreating side.

### Conclusions

An aeroacoustic method which is a combination of an aerodynamic method based on the flexible grid approach with acoustic integral methods for the prediction of HSI noise of helicopter rotors in forward flight is presented. The method is applied to two test cases.

The first test case is the ONERA/ECF 7AD rotor in high-speed forward flight as it was measured in the S1 Modane wind tunnel. Comparisons of aerodynamic blade pressure data show a good correlation with the measured pressure. Additionally a good agreement to numerical results of other authors is achieved.

The same rotor with different test conditions defined in the HELISHAPE project is used for aerodynamic and acoustic comparisons of the present method with experimental data measured in the DNW. The correlation of the blade pressure is less satisfactory compared to the first test case.

Based on the aerodynamic flowfield data of the second test case acoustic integral methods are applied to predict the pressure disturbance at the farfield. Additionally aerodynamic data of a non-lifting computation is used as input. For off-plane microphones a better agreement with experimental data is obtained by taking into account the correct blade loadings based on the prescribed blade motion. In contrast to this, a negative peak value independent on the rotor thrust is found for in-plane microphones.

The overall differences to the experimental data are caused by different reasons. Applying the linear acoustic analogy method neglects non-linear effects in the flowfield. The Kirchhoff method with a rotating integration surface is connected with the restriction of a subsonic integration surface. Therefore, the present conditions at moderate high-speed forward flight does not allow to include all transonic effects inside the Kirchhoff surface. The Kirchhoff method with a non-rotating integration surface requires accurate aerodynamic data at the Kirchhoff surface, which can not be obtained with the present coarse grid. Grid refinements promise to improve the results.

### Acknowledgment

The experimental aerodynamic and acoustic data of the ONERA/ECF 7AD rotor used for the comparative studies of the second test case was measured in the framework of the HELISHAPE project funded by the European Community under the BRI-TE/EURAM Program. For the first test case experimental data was kindly provided by ONERA.

### References

- [1] K. Pahlke and J. Raddatz. Flexibility Enhancement of Euler Codes for Rotor Flows by Chimera Techniques. *Paper No. 35, 20th European Rotorcraft Forum, Amsterdam, 1994.*
- [2] J. Ahmad and E.P.N. Duque. Helicopter Rotor Blade Computation in Unsteady Flows using Moving Embedded Grids. *AIAA 94-1922, 1994.*
- [3] J.-C. Boniface, B. Mialon, and J. Sidès. Numerical Simulation of Unsteady Euler Flow Around Multibladed Rotor in Forward Flight Using a Moving Grid Approach. *51th Annual Forum of the American Helicopter Society, Fort Worth, TX, May 9-11, 1995.*
- [4] J.-C. Boniface and K. Pahlke. Calculations of Multibladed Rotors in Forward Flight Using 3-D Euler Methods of DLR and ONERA. *Paper No. 58, 22nd European Rotorcraft Forum, Brighton, UK, 1996.*
- [5] F.H. Schmitz, D.A. Boxwell, W.R. Spletstösser, and W. Schultz. Model Rotor High-Speed Impulsive Noise: Full-Scale Comparisons and Parametric Variations. *Vertica, Vol.8, No.4, pp.395-422, 1984.*
- [6] R.C. Strawn, R. Biswas, and A.S. Lyrintzis. Helicopter Noise Predictions using Kirchhoff Methods. *51th Annual Forum of the American Helicopter Society, Fort Worth, TX, May 9-11, 1995.*
- [7] M. Kuntz. Rotor Noise Predictions in Hover and Forward Flight Using Different Aeroacoustic Methods. *AIAA 96-1695, 1996.*
- [8] K. Brentner, A.S. Lyrintzis, and E.K. Koutsavdis. A Comparison of Computational Aeroacoustic Prediction Methods for Transonic Rotor Noise. *52th Annual Forum of the American Helicopter Society, Washington, 1996.*
- [9] J. Ahmad, E.P.N. Duque, and R.C. Strawn. Computations of Rotorcraft Aeroacoustics with a Navier-Stokes/Kirchhoff Method. *Paper No.51, 22nd European Rotorcraft Forum, Brighton, UK, 1996.*

- [10] P. Beaumier, M. Costes, and R. Gaveriaux. Comparison between FP3D Full Potential Calculations and S1 Modane Wind Tunnel Test Results on Advanced Fully Instrumented Rotors. *Paper No. C12, 19th European Rotorcraft Forum, Como, 1993.*
- [11] K.-J. Schultz, W. Spletstösser, B. Junker, W. Wagner, E. Schoell, E. Mercker, K. Pengel, G. Arnaud, and D. Fertis. A Parametric Wind Tunnel Test on Rotorcraft Aerodynamics and Aeroacoustics (HELISHAPE) - Test Procedures and Representative Results. *Paper No. 52, 22nd European Rotorcraft Forum, Brighton, UK, 1996.*
- [12] N. Kroll, R. Radespiel, and C.-C. Rossow. Accurate and Efficient Flow Solver for 3D Applications on Structured Meshes. *Lecture Series 1994, Computational Fluid Dynamics, Von Karman Institute of Fluid Dynamics, 1994.*
- [13] A. Jameson, W. Schmidt, and E. Turkel. Numerical Solutions of the Euler Equations by Finite Volume Methods Using Runge-Kutta Time-Stepping Schemes. *AIAA 81-1259, 1981.*
- [14] A. Jameson. Time Dependent Calculation using Multigrid, with Applications to Unsteady Flows past Airfoils and Wings. *AIAA 91-1596, 1991.*
- [15] R. Heinrich, K. Pahlke, and H. Bleecke. A Three Dimensional Dual-Time Stepping Method for the Solution of the Unsteady Navier-Stokes Equation. *Unsteady Aerodynamics, Royal Aeronautical Society, London, 1996.*
- [16] N. Kroll. Berechnung der Strömungsfeldgrößen um Propeller und Rotoren im Schwebeflug durch die Lösung der Euler-Gleichungen. *DLR FB 89-37, 1989.*
- [17] D. Lohmann. Prediction of Ducted Radiator Fan Aeroacoustics With a Lifting Surface Method. *AIAA-92-02-098, 14th Aeroacoustic Conference, No. 2, pp. 576-606, Aachen, May, 1992.*
- [18] K.J. Schultz, D. Lohmann, J.A. Lieser, and K. Pahlke. Aeroacoustic Calculations of Helicopter Rotors at DLR. *Paper No. 29, AGARD Symposium on Aerodynamics and Aeroacoustics of Rotorcraft, Berlin, Oct.10-14, 1994.*
- [19] M. Kuntz, D. Lohmann, J.A. Lieser, and K. Pahlke. Comparisons of Rotor Noise Predictions obtained by a Lifting Surface Method and Euler Solutions using Kirchhoff Equation. *CEAS/AIAA 95-136, 1995.*
- [20] F. Farassat and G.P. Succi. The Prediction of Helicopter Rotor Discrete Frequency Noise. *Vertica, Vol. 7, No. 4, pp. 309-320, 1983.*
- [21] K.S. Brentner. Prediction of Helicopter Rotor Discrete Frequency Noise. *NASA Technical Memorandum 87721, 1986.*
- [22] F. Farassat and M.K. Myers. Extension of Kirchhoffs Formula to Radiation from Moving Surfaces. *Journal of Sound and Vibration, Vol. 123(3), pp. 451-460, 1988.*
- [23] A.S. Lyrantzis. The Use of Kirchhoff Method in Computational Aeroacoustics. *ASME Journal of Fluids Engineering, Dec. 1994.*
- [24] K. Brentner. Numerical Algorithms for Acoustic Integrals - The Devil is in the Details. *AIAA 96-1706, 1996.*
- [25] T. Schwarz. Berechnung der Umströmung einer Hubschrauber-Rotor-Rumpf-Konfiguration auf Basis der Euler-Gleichungen mit der Chimären-Technik. *Studienarbeit, DLR Braunschweig, 1997.*

Figures

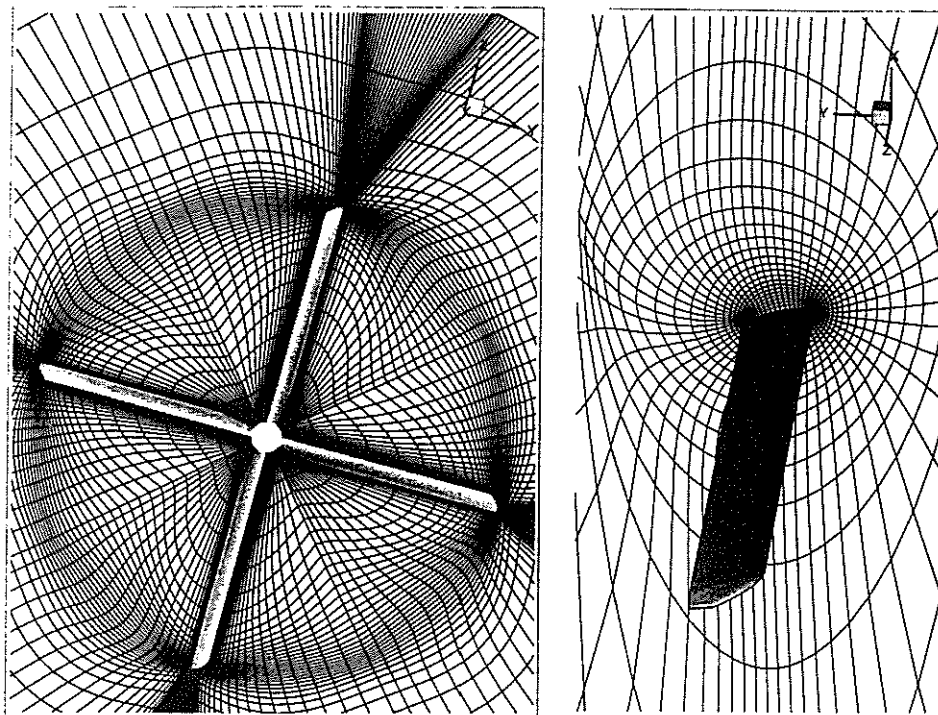


Figure 3: ONERA/ECF 7AD rotor, view of 4-block grid system (rotor plane and blade)

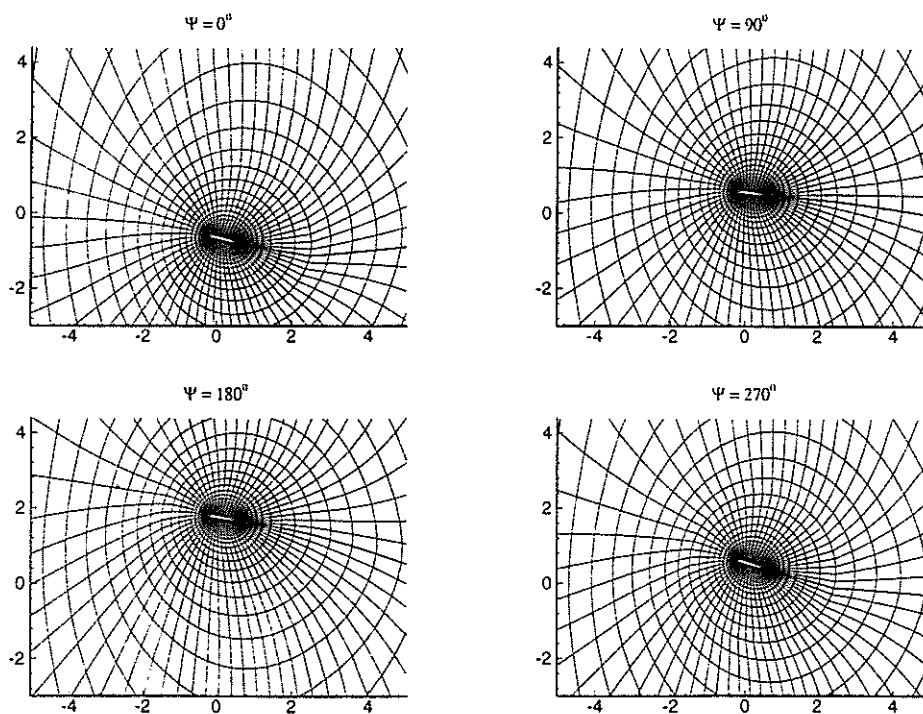


Figure 4: ONERA/ECF 7AD rotor, view of grid plane at  $r/R=0.9$

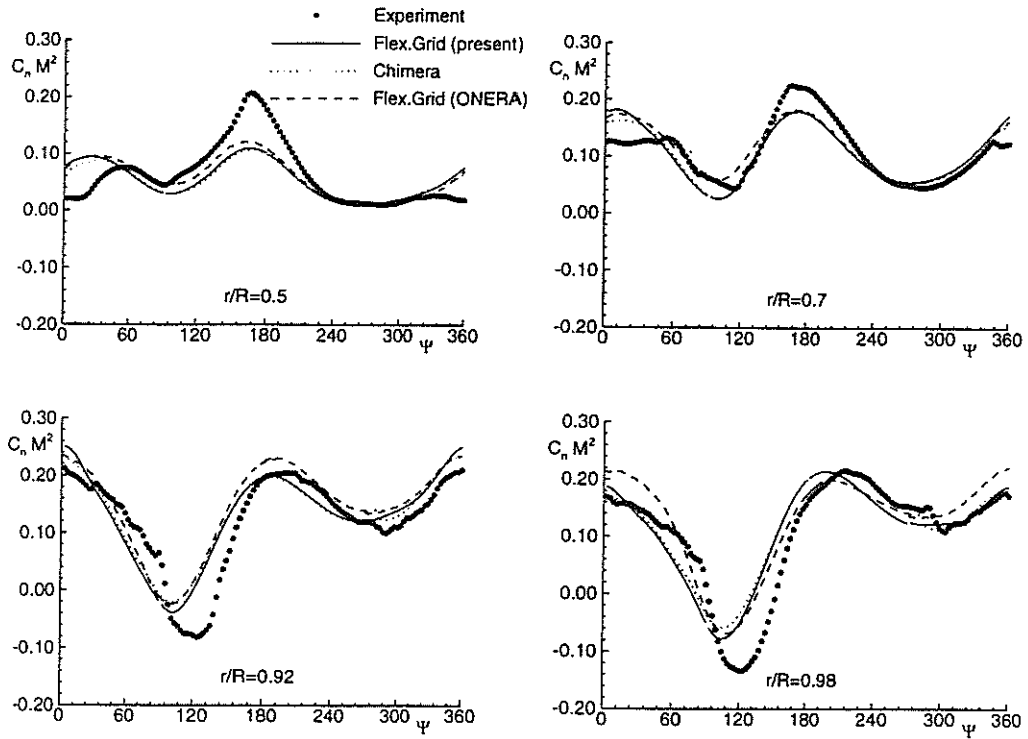


Figure 5: ONERA/ECF 7AD rotor comparison of  $C_n M^2$  (S1 test case,  $M_{\omega R} = 0.617$ ,  $\mu = 0.4$ )

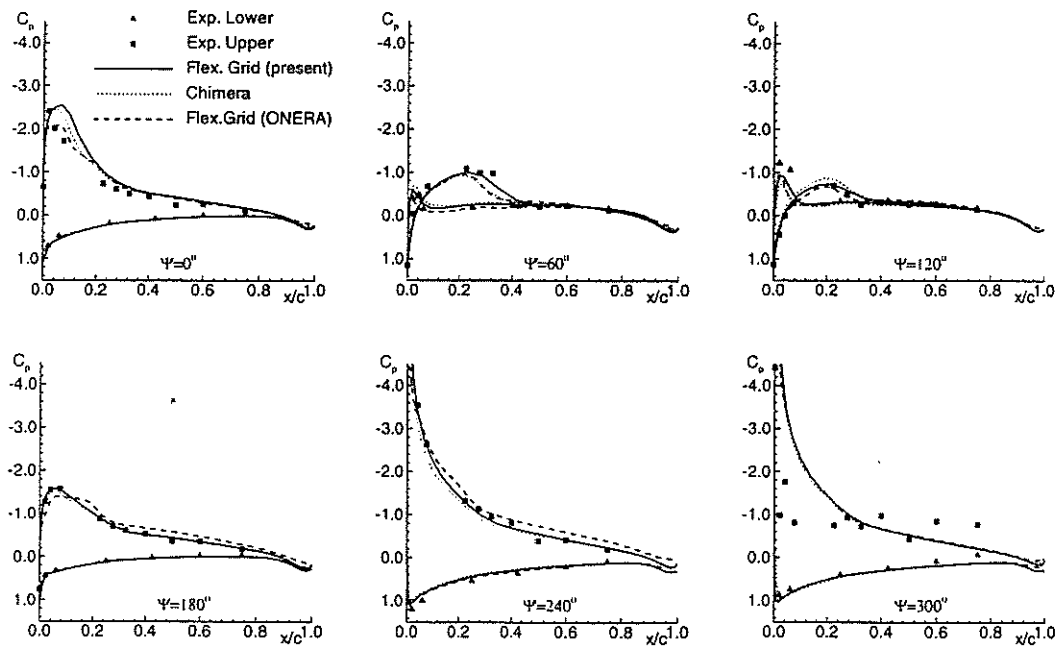


Figure 6: ONERA/ECF 7AD rotor. comparison of pressure coefficient at  $r/R=0.92$  (S1 test case,  $M_{\omega R} = 0.617$ ,  $\mu = 0.4$ )

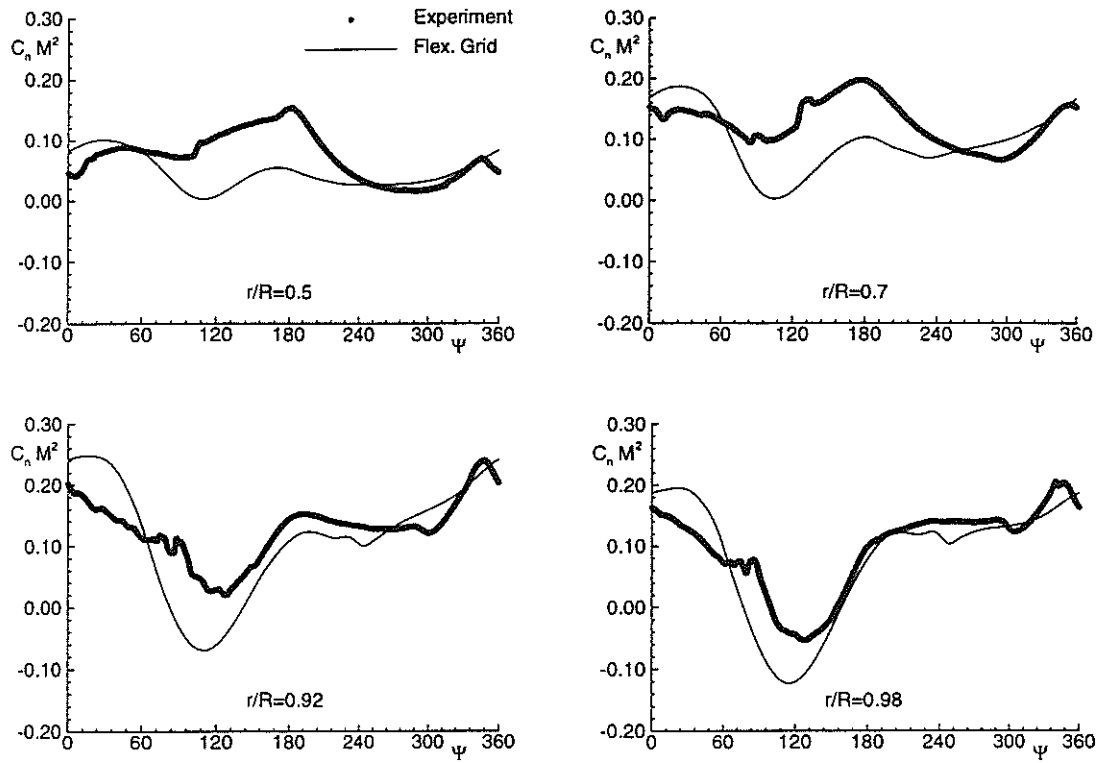


Figure 7: ONERA/ECF 7AD rotor, comparison of  $C_n M^2$  (DNW test case,  $M_{\omega R} = 0.6604$ ,  $\mu = 0.3276$ )

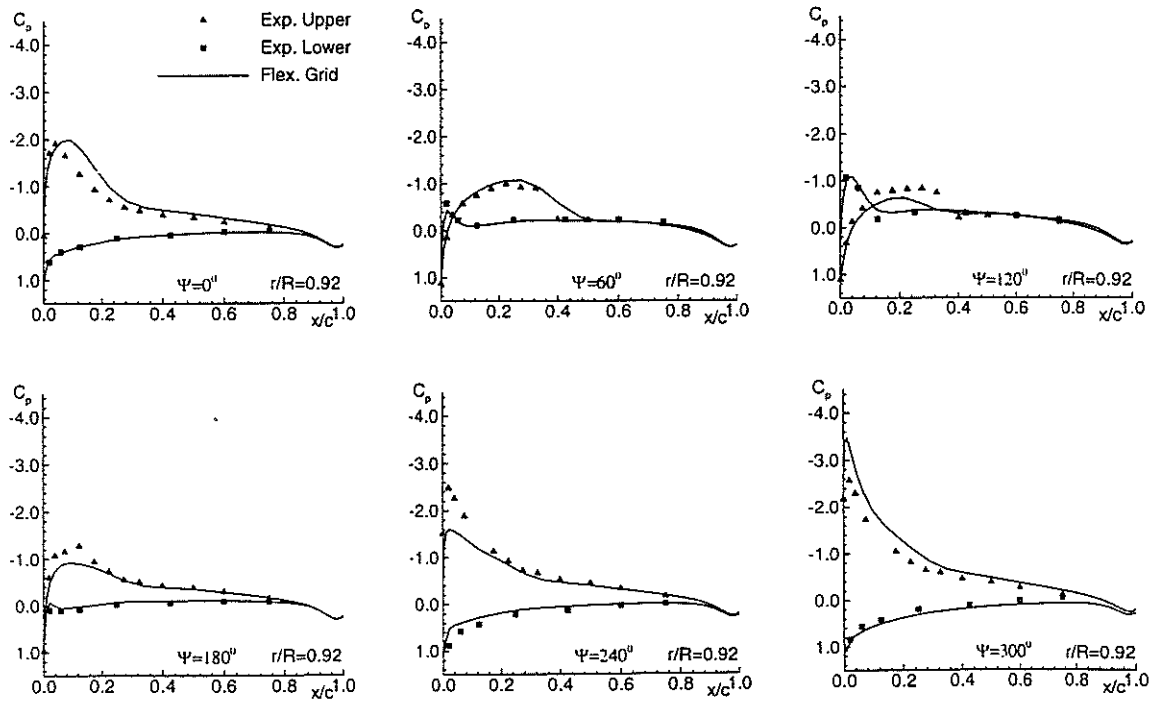


Figure 8: ONERA/ECF 7AD rotor, comparison of pressure coefficient at  $r/R=0.92$  (DNW test case,  $M_{\omega R} = 0.6604$ ,  $\mu = 0.3276$ )

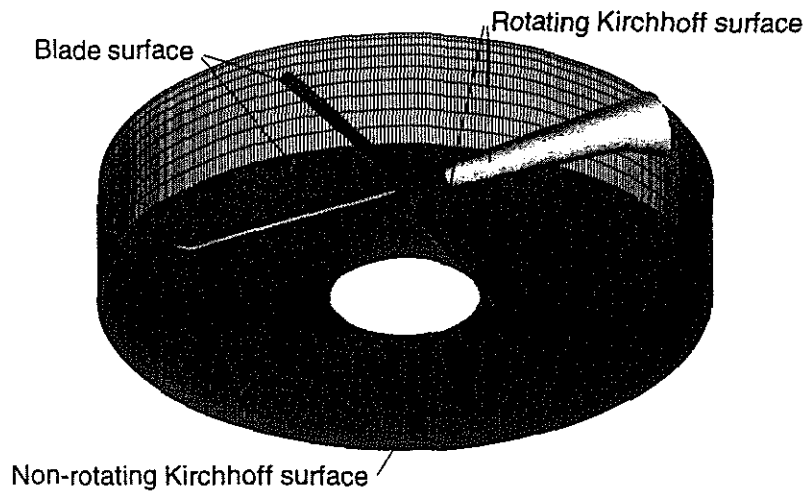


Figure 9: ONERA/ECF 7AD rotor, view of blade surfaces and Kirchhoff grids

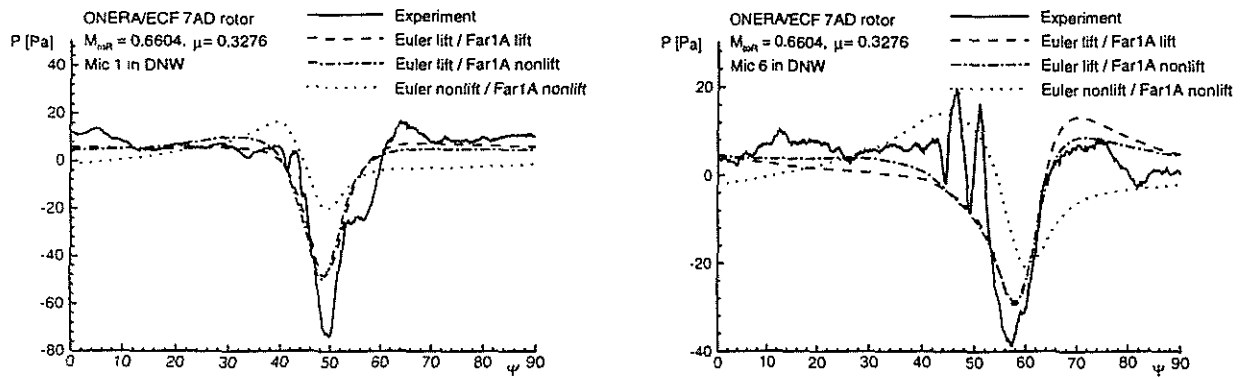


Figure 10: ONERA/ECF 7AD rotor, influence of lifting/non-lifting aerodynamic data on pressure signature for linear acoustic analogy method (DNW test case,  $M_{\infty R} = 0.6604$ ,  $\mu = 0.3276$ ),

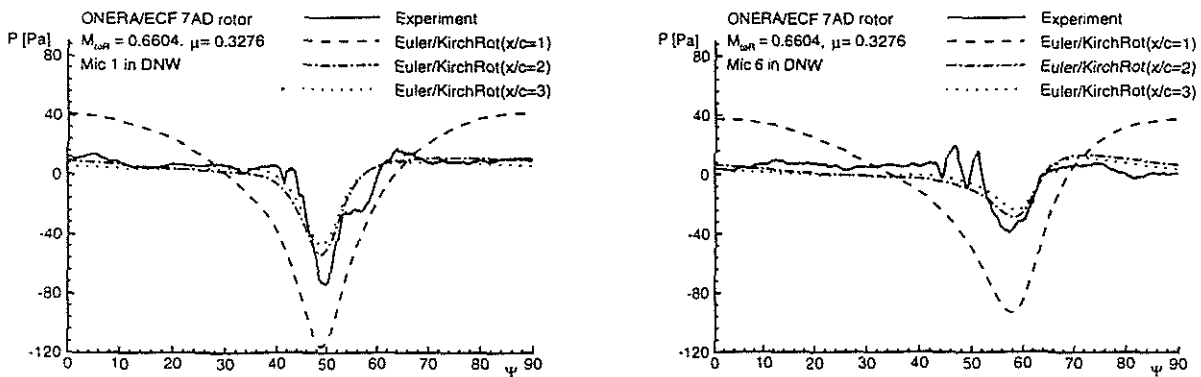


Figure 11: ONERA/ECF 7AD rotor, Kirchhoff surface location variations for rotating Kirchhoff formalism (DNW test case,  $M_{\infty R} = 0.6604$ ,  $\mu = 0.3276$ ),

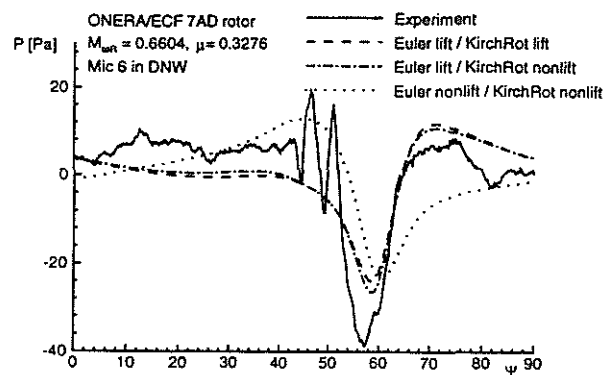
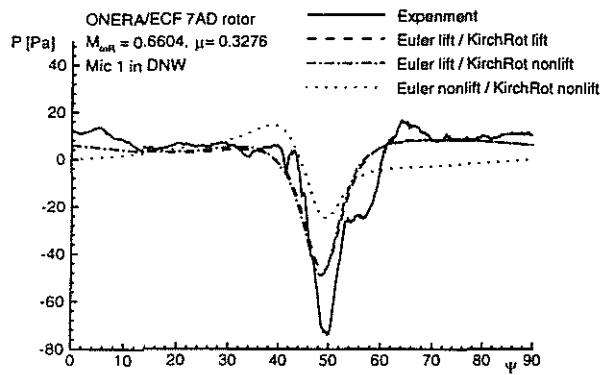


Figure 12: ONERA/ECF 7AD rotor, influence of lifting/non-lifting aerodynamic data on pressure signature for rotating Kirchhoff method (DNW test case,  $M_{\omega R} = 0.6604$ ,  $\mu = 0.3276$ ),

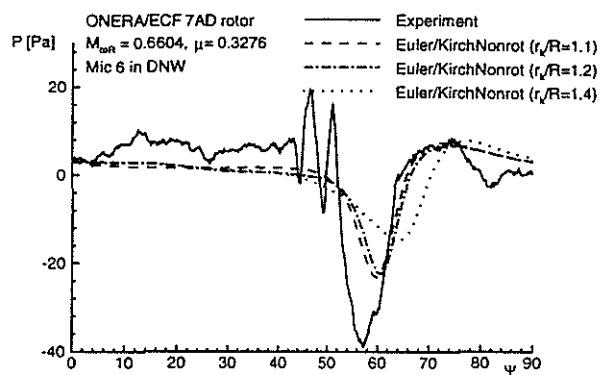
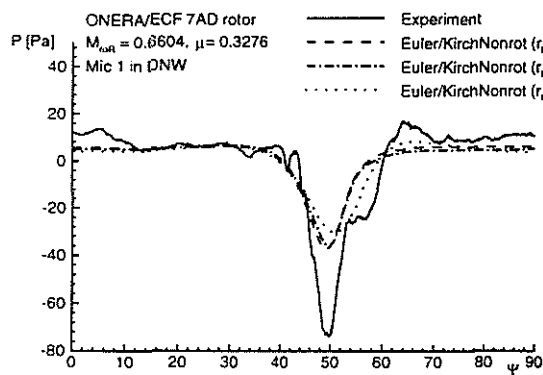


Figure 13: ONERA/ECF 7AD rotor, Kirchhoff surface location variations for non-rotating Kirchhoff formalism (DNW test case,  $M_{\omega R} = 0.6604$ ,  $\mu = 0.3276$ ),

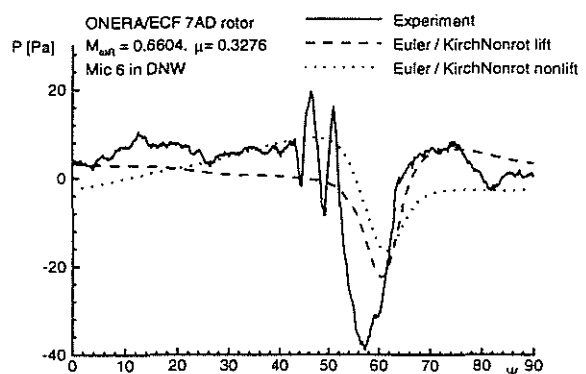
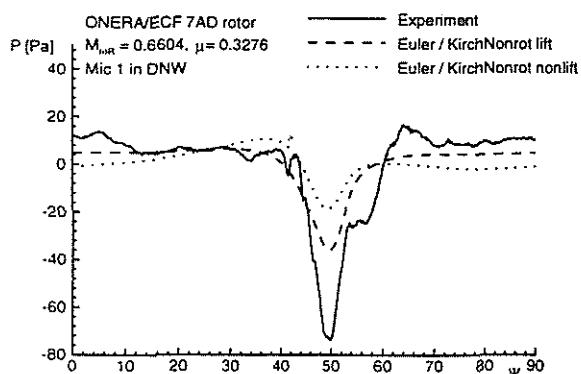


Figure 14: ONERA/ECF 7AD rotor, influence of lifting/non-lifting aerodynamic data on pressure signature for non-rotating Kirchhoff method (DNW test case,  $M_{\omega R} = 0.6604$ ,  $\mu = 0.3276$ ),

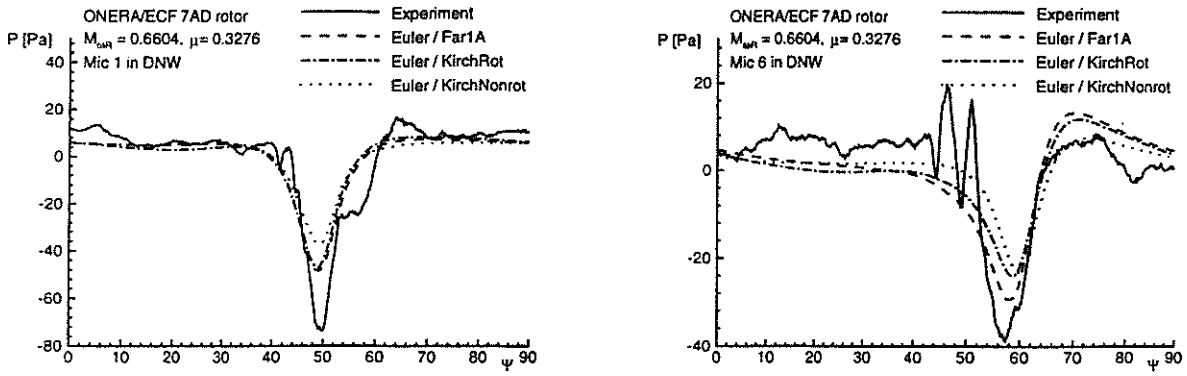


Figure 15: ONERA/ECF 7AD rotor, comparison of pressure signatures for different acoustic methods (DNW test case,  $M_{\omega R} = 0.6604$ ,  $\mu = 0.3276$ ),

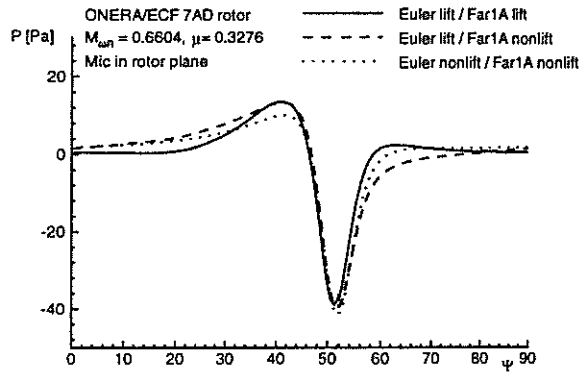


Figure 16: ONERA/ECF 7AD rotor, influence of lifting/non-lifting aerodynamic data on pressure signature at in-plane microphone for linear acoustic analogy method (DNW test case,  $M_{\omega R} = 0.6604$ ,  $\mu = 0.3276$ ),

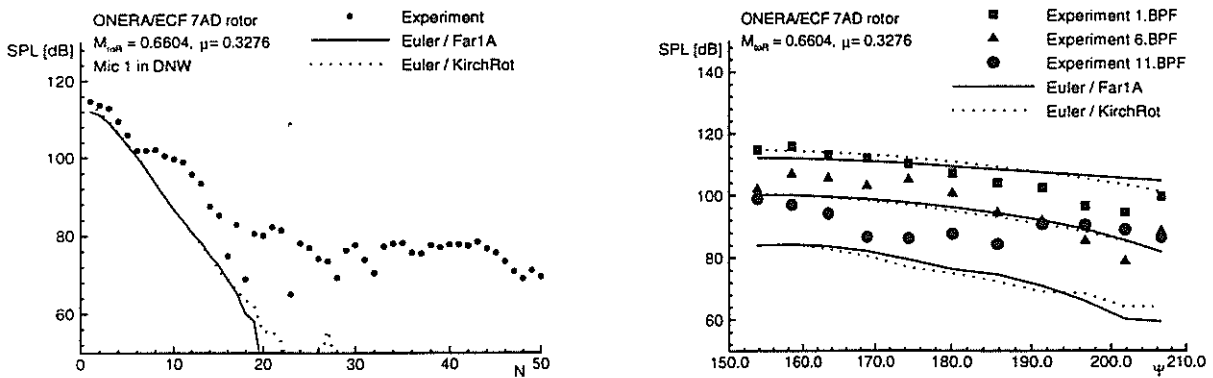


Figure 17: ONERA/ECF 7AD rotor, comparison of sound pressure level (DNW test case,  $M_{\omega R} = 0.6604$ ,  $\mu = 0.3276$ ),